Inorg. Chem. **2003**, *42*, 2014–2023

Molecular Precursors for Ferroelectric Materials: Synthesis and Characterization of $Bi_2M_2(\mu\text{-}O)(sal)_4(Hsal)_4(OEt)_2$ and $BiM_4(\mu\text{-}O)_4(sal)_4(Hsal)_3(O^iPr)_4$ (sal = $O_2CC_6H_4O$, Hsal = $O_2CC_6H_4OH$) (M = Nb, Ta)

John H. Thurston and Kenton H. Whitmire*

Department of Chemistry, MS-60, Rice University, 1600 Main Street, Houston, Texas 77005

Received October 14, 2002

Reactions between triphenyl bismuth, salicylic acid, and niobium or tantalum ethoxide have been explored. Four new coordination complexes incorporating bismuth and the group 5 metals niobium or tantalum have been synthesized and characterized spectroscopically, by elemental analysis, and by single crystal X-ray diffraction. The new complexes are $Bi_2M_2(\mu\text{-}O)(sal)_4(Hsal)_4(OEt)_2$ (**1a**, M = Nb; **1b**, M = Ta) and $BiM_4(\mu\text{-}O)_4(sal)_4(Hsal)_3(O^iPr)_4$ (sal = $O_2CC_6H_4$-2-O, Hsal = $O_2CC_6H_4$-2-OH) (**2a**, M = Nb; **2b**, M = Ta). Complexes **1a** and **1b** are isomorphous, as are **2a** and **2b**. The thermal and hydrolytic decomposition of **1a** has been explored by DT/TGA and powder X-ray diffraction, while scanning electron microscopy (SEM) and energy dispersive X-ray spectroscopy (EDX) were used to characterize the morphology and composition of the oxides. The heterobimetallic molecules are completely converted to the amorphous bimetallic oxide by heating to 500 °C in air. Decomposition of **1a** or **1b** at 650 °C produces the metastable high temperature form of $BiNbO_4$ as the major crystalline oxide phase. Heating samples of **1a** to 850 °C favors conversion of the materials to the low temperature phase as well as disproportionation into $Bi_5Nb_3O_{15}$ and Nb_2O_5. Thermal decomposition of **1a** and **1b** produces porous oxides, while hydrolytic decompostion of the complexes has been shown to produce nanometer scale bimetallic oxide particles. The potential of the complexes to act as single-source precursors for ferroelectric materials is considered.

Introduction

Ferroelectric materials are currently being heavily investigated for the development of new piezoelectric, pyroelectric, and optoelectronics devices,[1] and in particular, materials that show the properties of nonvolatility, spontaneous polarization, and a high dielectric constant are highly desirable. These properties have prompted exploration of ferroelectric materials for the formation of nonvolatile random access memories (NVRAM), either alone or in conjunction with current silicon-based technology.[1] One of the major shortcomings of many of these materials is the fact that they tend to exhibit significant fatigue when exposed to repeat electronic cycling.[2] This fatigue has been attributed to reduction of some of the Ti^{4+} ions to Ti^{3+} and consequent defect formation in the oxide lattice.[3,4] The incorporation of niobium or tantalum into ferroelectric oxides has been reported to be extremely effective in reducing the fatigue typically experienced by the material under repeated cycling.[2,4] Thin films of the binary oxides $BiNbO_4$ are particularly interesting because they are ferroelectric when the thickness of the oxide film is less than 250 nm, while thicker layers are antiferroelectric.[5,6] Thin films of the oxide $BiTaO_4$ have also recently been shown to demonstrate ferroelectric properties.[7] Both of these materials may be resistant to the problems that plague some of the titanium-based oxides that are commonly used today.

* Author to whom correspondence should be addressed. E-mail: whitmir@rice.edu. Phone: 713-348-5650. Fax: 713-348-5155.

(1) *Science and Technology of Electroceramic Thin Films*; Auciello, O., Waser, R., Eds.; Kluwer Academic Publishers: Dordrecht, The Netherlands, 1995.
(2) Watanabe, H.; Mihara, T.; Yoshimori, H.; Paz de Araujo, C. *Jpn. J. Appl. Phys.* **1995**, *34*, 5240−5244.
(3) Warren, W. L.; Dimos, D.; Tuttle, B. A.; Nasby, R. D.; Pike, G. E. *Appl. Phys. Lett.* **1994**, *65*, 1018−1020.
(4) Du, X.; Chen, I. *Mater. Res. Soc. Symp. Proc.* **1998**, *493*, 261−266.
(5) Chattopadhyay, S.; Ayyub, P.; Pinto, R.; Multani, M. S. *J. Mater. Res.* **1998**, *13*, 1113−1116.
(6) Ayyub, P.; Chattopadhyay, S.; Pinto, R.; Multani, M. S. *Phys. Rev. B* **1998**, *57*, R5559−R5562.
(7) Vorotilov, K. A.; Sigov, A. S.; Turevskaya, E. P.; Bergo, V. B.; Sokolov, S. V. *Russ. Microelectron.* **1999**, *28*, 161−167.

10.1021/ic026108s CCC: $25.00
Published on Web 02/08/2003

Molecular precursors that are compatible with traditional methods of thin and thick oxide film synthesis such as metal−organic chemical vapor deposition (MOCVD), sol−gel deposition, laser ablation, and metal−organic decomposition (MOD) are attractive routes to the formation of these electronic materials, where the use of single-source precursors may afford control of the metal stoichiometry in the final product.[8] Molecular precursors produce exceptionally homogeneous materials due to the intimate mixing of the metals at the molecular level.[9] Further, the presence of bridging or chelating organic ligands in molecular complexes has been shown to successfully arrest unwanted metal segregation during oxide formation.[10] In addition, the loss of organic volatile material during calcination may impart unusual or desirable structural features on the product material, such as high surface area, low density, connected channels, or the formation of metastable phases. The use of well-defined bimetallic precursors has been observed to produce crystalline oxides under conditions that are significantly milder than those employed in traditional solid-state syntheses.[11,12]

For these reasons, we have chosen to explore the synthesis and chemistry of bismuth−group 5 transition metal complexes as potential single-source molecular precursors for the formation of ferroelectric materials. We have recently reported on the synthesis and thermal decomposition studies of the heterometallic salicylate complexes $Bi_2M_2(sal)_4(Hsal)_4(OR)_4$ (M = Nb, Ta; R = CH_2CH_3, $CH(CH_3)_2$), $Bi_2Ti_3(sal)_8(Hsal)_2$, and $Bi_2Ti_4(O^iPr)(sal)_{10}(Hsal)$ (sal = $O_2CC_6H_4$-2-O; Hsal = $O_2CC_6H_4$-2-OH).[12] We report here the synthesis and characterization of new heterometallic bismuth−group 5 metal complexes that incorporate oxide ions. These include $Bi_2M_2(\mu\text{-}O)(sal)_4(Hsal)_4(OEt)_2$ (**1a**, M = Nb; **1b**, M = Ta) and $BiM_4(\mu\text{-}O)_4(sal)(Hsal)(O^iPr)_4$ (**2a**, M = Nb; **2b**, M = Ta). The complexes have been characterized spectroscopically and by single crystal X-ray diffraction. The decomposition of **1** through pyrolysis and hydrolysis has been investigated using powder X-ray diffraction, thermogravimetric analysis/differential thermal analysis (TGA/DTA), scanning electron microscopy (SEM), energy dispersive X-ray spectroscopy (EDX), and Brunauer, Emmett, and Teller (BET) surface area measurements. The formation of the material $BiMO_4$ (M = Nb, Ta) from the decompostion of **1a** and **1b** has been confirmed.

Experimental Section

All synthetic reactions were carried out using standard Schlenk or glovebox techniques under an atmosphere of purified nitrogen or argon. Solvents were purified over an appropriate reagent under argon and were distilled immediately prior to use.[13] Niobium ethoxide, tantalum ethoxide (Strem), salicylic acid, HPLC grade water and tetraethylammonium hydroxide (Aldrich Chemical Co.) were used without further purification. Magnesium acetate (Aldrich Chemical Co.) was dehydrated by refluxing in acetic anhydride for 24h.[10] All elemental analyses were performed by Galbraith Laboratories. Multinuclear NMR studies were performed on a Bruker 200 MHz, a Bruker 400 MHz, or a Bruker 500 MHz Avance instrument and referenced to the protio imputity in the deuterated solvent (^{1}H), or to the solvent signal (^{13}C). Chemical shifts are reported in parts per million (ppm), while coupling constants are reported in hertz (Hz). Coupling constants were generally not resolved for the aromatic protons in the molecules discussed in this paper, except as noted. The following abbreviations are used: s − singlet, d − doublet, t − triplet, q − quartet, sp − septet, br − broad, Ar − aromatic. ^{13}C NMR studies did not resolve the *ipso* carbon of the salicylate ligand, even with extended collection times. This has been attributed to the quaternary nature and consequent very short relaxation time of this atom. TGA studies were performed on a Sieko DT/TGA 200 instrument in platinum pans under an oxygen-containing atmosphere. Approximately 5 mg of the sample to be studied was placed in a platinum pan in the furnace of a Sieko TGA/DTA instrument. The sample was heated to 600 °C at a rate of 10 °C per minute in air. Phase changes in the molecular precursor that occurred during thermal decomposition were monitored by DTA. Powder X-ray diffraction studies were performed on a Siemens Diffraktometer using Cu Kα radiation (λ = 1.5418 Å). Data were collected on 2θ in the range 22° to 36° in 0.05° increments at 15 s per frame. Data processing of the powder diffraction results and phase identification was accomplished using the program JADE.[14] The morphologies and relative compositions of the oxides produced through pyrolysis and hydrolysis were examined on a FEI XL30 Schottky field-emission environmental scanning electron microscope (SEM) with an energy-dispersive X-ray spectroscopy (EDX) attachment. Samples were studied using a 30kV acceleration voltage and a spot size setting of 3. Surface area measurements of the oxides of **1a** and **1b** were conducted on a Coulter SA3100 instrument using the five-point method of Brunauer, Emmett and Teller (BET). Solution-state molar mass studies of **1b** were performed according to the literature procedures,[15] using dichloromethane as a solvent and tetraphenyl lead(IV) as a standard.

Synthesis

$Bi_2M_2(\mu\text{-}O)(sal)_4(Hsal)_4(OEt)_2$ (1a, M = Nb; 1b, M = Ta). Due to the similarity in the syntheses of these complexes, a general procedure is presented here. Triphenyl bismuth (0.440 g, 1.0 mmol) and salicylic acid (1.1 g, 8 mmol) were suspended in toluene (20 mL) under an atmosphere of argon. The suspension was refluxed for 1 h, and then cooled to room temperature. Dropwise addition of niobium ethoxide (0.24 mL, 1.0 mmol) to the yellow bismuth salicylate resulted in dissolution of the solid followed by rapid formation of a yellow precipitate. The suspension was stirred at room temperature for 24 h, and the solvent was removed under reduced pressure. The crude product was washed with diethyl ether (2 × 10 mL), dried under vacuum, and recrystallized from dichloromethane and hexane to afford bright yellow crystals. Compound **1a**: yield, 0.62 g (0.34 mmol, 69%); ^{1}H NMR (C_6D_6), 0.92 (t, CH_3, 3H, J_{H-H} = 4.1 Hz), 3.3 (q, CH_2, 2H, J_{H-H} = 4.1

(8) *Piezoelectric Ceramics*; Jaffe, B., Cook, W. R., Jaffe, H., Eds.; Academic Press: London, 1971; Vol. 3.
(9) Annika, I.; Pohl, M.; Westin, L. G.; Kritikos, M. *Chem. Eur. J.* **2001**, *7*, 3438−3445.
(10) Boulmaaz, S.; Papiernik, R.; Hubert-Pfalzgraf, L. G.; Spete, B.; Vaissermann, J. *J. Mater. Chem.* **1997**, *7*, 2053−2061.
(11) Chae, H. K.; Payne, D. A.; Xu, Z.; Ma, L. *Chem. Mater.* **1994**, *6*, 1589−1592.
(12) Thurston, J. H.; Whitmire, K. H. *Inorg. Chem.* **2002**, *41*, 4194−4205.
(13) Armarego, W. L. F.; Perry, D. D. *Purification of Laboratory Chemicals*, 4th ed.; Butterworth-Heinemann: Boston, 1996.
(14) *JADE, XRD Pattern-Processing for the PC 2.1*; MDI: Livermore, CA, 1994.
(15) Francis, J. A.; McMahon, C. N.; Bott, S. G.; Barron, A. R. *Organometallics* **1999**, *18*, 4399−4416.

Hz), 6.5 (s, Ar*H*), 6.7 (s, Ar*H*), 6.9 (s, Ar*H*), 7.8 (s, Ar*H*); ^{13}C-{^{1}H} NMR (C_6D_6), 30.6 (*C*H$_3$), 57.8 (*C*H$_2$), 118.6 (ArC), 119.7 (ArC), 129.7 (ArC), 131.7 (ArC), 136.9 (*C*OH), 162.8 (*C*O$_2$); elemental anal. (% calcd for $Bi_2Nb_2C_{60}H_{46}O_{27}$), C 40.08 (39.97), H 2.82 (2.57); IR, 3187, 1645, 1622, 1599, 1577, 1531, 1456, 1385, 1349, 1309, 1221, 1157, 1141, 1095, 1063, 897, 872, 827, 805, 757, 726, 702; TGA(%) obsd (calcd for formation of $BiNbO_4$), 60.4 (61.5). Compound **1b**: yield, 0.58 g (0.30 mmol, 58%); ^{1}H NMR (C_6D_6), 0.88 (t, C*H*$_3$, 3H, J_{H-H} = 7.2 Hz), 3.3 (q, C*H*$_2$, 2H, J_{H-H} = 7.2 Hz), 6.5 (s, Ar*H*), 6.9 (s, Ar*H*), 7.0 (s, Ar*H*), 7.8 (s, Ar*H*); ^{13}C{^{1}H}NMR (C_6D_6), 21.8 (*C*H$_3$), 57.4 (*C*H$_2$), 118.5 (ArC), 119.7 (ArC), 127.9 (ArC), 129.7 (ArC), 131.6 (ArC), 137.0 (*C*OH), 163.1 (*C*O$_2$), elemental anal. (%) obsd (calcd for $Bi_2Ta_2C_{60}H_{46}O_{27}$), C 35.74 (36.08), H 2.48 (2.43); IR, 3182, 1601, 1578, 1543, 1498, 1458, 1384, 1350, 1315, 1240, 1142, 1115, 1081, 1032, 899, 871, 854, 835, 804, 756, 732; TGA (%) obsd (calcd for formation of $BiTaO_4$), 55.0 (54.5).

BiM$_4$(μ-O)$_4$(Hsal)$_3$(sal)$_4$(O^{i}Pr)$_4$ (2a, M = Nb; 2b, M = Ta). Similarly to **1a** and **1b**, the procedures for production of **2a** and **2b** are almost identical, and only one is given. Triphenyl bismuth (0.440 g, 1.0 mmol) and salicylic acid (3.0 g, 22 mmol) were refluxed in toluene for 1 h to give a clear colorless solution. The solvent was removed under reduced pressure, and the yellow residue was redissolved in 5 mL of 2-propanol to give a clear, very pale yellow solution. Solid magnesium acetate (0.142 g, 1.0 mmol) was introduced, and the solution became colorless. Dropwise addition of niobium ethoxide (0.48 mL, 2.0 mmol) to the mixture resulted in a clear yellow solution that was allowed to stand for 14 days at room temperature. During this time, yellow cubic crystals deposited in the flask along with a white solid. X-ray quality crystals were taken directly from the reaction mixture. The bright yellow and white solids were isolated by filtration. Since the white compound is insoluble in dichloromethane, the yellow compound could be separated from it by dissolution in dichloromethane and filtration through a bed of dry Celite. The product was isolated via the addition of hexane to the filtrate to produce bright yellow crystals. The crystals were collected by filtration, washed with diethyl ether (1 × 10 mL), dried in vacuo, and stored under nitrogen. Compound **2a**: yield, 0.52 g (2.83 mmol, 57% based on niobium); ^{1}H NMR (C_6D_6), 0.92 (d, C*H*$_3$, 6H, J_{H-H} = 4.2 Hz), 3.7 (h, C*H*, 1H, J_{H-H} = 4.2 Hz), 6.5 (t, Ar*H*), 6.9 (d, Ar*H*), 7.1 (td, Ar*H*), 7.7 (d, Ar*H*); ^{13}C{^{1}H} NMR (C_6D_6), 25.5 (CH_3), 62.4 (CH_2), 118.5 (Ar*C*), 119.8 (Ar*C*), 129.7 (Ar*C*), 131.3 (Ar*C*), 137.2 (*C*OH), 163.3 (*C*O$_2$); IR, 3231, 1655, 1593, 1542, 1463, 1392, 1250, 1156, 1110, 1007, 895, 869, 803, 746; elemental anal. % obsd (% calcd for $BiNb_4C_{61}H_{60}O_{29}$), C 39.17 (39.89), H 3.22 (3.24). Compound **2b**: yield, 0.68 g (3.11 mmol, 62% based on tantalum); ^{1}H NMR (C_6D_6), 0.91 (d, C*H*$_3$, 6H, J_{H-H} = 7.0 Hz), 3.31 (h, C*H*, 1H, J_{H-H} = 6.9 Hz), 6.498 (br s, Ar*H*), 6.927 (br d, Ar*H*), 7.049 (br s, Ar*H*), 7.736 (s, O*H*); ^{13}C-{^{1}H}NMR (C_6D_6), 21.771 (*C*H$_3$), 57.431 (*C*H), 118.505 (Ar*C*), 119.738 (Ar*C*), 127.914 (Ar*C*), 129.671 (Ar*C*), 131.553 (Ar*C*), 137.041 (*C*OH), 163.064 (*C*O$_2$); IR, 3275, 1648, 1563, 1541, 1460, 1387, 1385, 1248, 1153, 1111, 1007, 890, 864, 801, 745; elemental anal. (%) obsd (calcd for $BiTa_4C_{61}H_{60}O_{29}$), C 32.75 (33.47), H 2.79 (2.72).

Pyrolysis of 1. A sample of the complex (approximately 0.25 g) was placed in a covered porcelain dish, loaded into a furnace at the desired temperature, and maintained at that temperature for 2−8 h. The sample was then slowly cooled to room temperature. The resulting oxide was ground in an agate mortar and pestle to produce a finely dispersed white or pale yellow powder that was used in powder X-ray diffraction studies.

Hydrolysis of 1. A three-neck 100-mL round-bottom flask was fitted with a condenser and 25-mL pressure-equalizing addition funnel. The round-bottom flask was loaded with 10 mL of HPLC grade water and 0.05 g of a 25% solution of tetraethylammonium hydroxide in methanol. Vigorous stirring was initiated, and the solution was heated to gentle reflux. A sample of the bimetallic complex (0.18 g, 0.1 mmol) was dissolved in 15 mL of anhydrous THF and placed into the addition funnel. The solution of the complex was introduced into the water dropwise. Hydrolysis of the molecular precursor occurred instantly, and the solution became turbid. After the addition of all of the THF solution, the addition funnel was removed, and the reaction mixture was refluxed for an additional 2 h to ensure completeness of reaction. After the reaction period, the mixture was allowed to cool to room temperature, and the solvent was decanted. The oxide was washed twice with THF/H_2O (1:1, 50 mL) and then once with H_2O (15 mL) to give the purified product. Scanning electron microscopy was used to examine samples of the oxide produced in this manner. EDX was used to confirm the presence of both metals in the particles.

Solid State Structure. Compounds **1**−**2** were studied on a Bruker Smart 1000 diffractometer equipped with a CCD area detector. The data were corrected for Lorentz and polarization effects. Absorption correction was applied using the program SADABS.[16] No appreciable decay of the crystals was detected during data collection. Heavy atoms in the compounds were located using direct methods with the SHELXTL software package.[17] All other atoms were located by successive Fourier difference maps and were refined using the full-matrix least-squares technique on F^2. All non-hydrogen atoms, with the discussed exceptions, were refined anisotropically. Hydrogen atoms in all of the complexes were placed in calculated positions and allowed to ride on the adjacent atom. Hydrogen atoms associated with phenolic oxygen atoms were placed in calculated positions and refined geometrically using a riding model. The hydrogen atom was oriented so that the most likely hydrogen bond, in this case to a carboxylate oxygen of the same molecule, was realized. Investigation of the packing structures of the molecules using the program PLATON[18] did not reveal the presence of intermolecular hydrogen bonds. Refinement of the model parameters against the observed data led to convergence. The following is a description for compounds **1a** and **1b**: These complexes were found to cocrystallize with three molecules of toluene. One of these solvent molecules lies on a C_2 axis, with the methyl group disordered over two positions in the crystal lattice. Attempts to resolve this disorder by transforming the crystallographic data to a space group that does not contain a mirror plane did not result in successful solution of the structure. Consequently, the toluene molecule was modeled with two methyl positions in a 1:1 ratio. Aromatic carbon−carbon bond lengths in the disordered lattice solvent were constrained to be equal. The disordered solvent molecule was refined isotropically. The following is a description for compounds **2a** and **2b**: The alkoxide functional groups of these molecules demonstrated significant motion in the solid-state. One of the groups in each complex was treated as being formally disordered, with partial occupancy of the methyl carbon atoms at three possible locations. The carbon atoms of the disordered alkoxide ligand were refined isotropically. The disorder was modeled with the three potential sites each allowed to contain two-thirds of a carbon atom. The distances between these three methyl

(16) Sheldrick, G. *SADABS 5.1*; University of Göttingen: Göttingen, Germany, 1997.
(17) Sheldrick, G. *SHELXTL 6.1*; University of Göttingen: Göttingen, Germany, 2001.
(18) Spek, A. L. *Platon, A Multipurpose Crystallographic Tool*; Utrecht University: Utrecht, The Netherlands, 2001.

Table 1. Crystallographic Data for New Compounds

	$C_{60}H_{46}Bi_2Nb_2O_{27}$	$C_{60}H_{46}Bi_2Ta_2O_{27}$	$C_{61}H_{60}BiNb_4O_{29}$	$C_{61}H_{60}BiTa_4O_{29}$
fw	2091.12	2269.21	1835.69	2186.85
space group	*C*2/*c*	*C*2/*c*	$P2_1/n$	$P2_1/n$
Z	4	4	4	4
cryst syst	monoclinic	monoclinic	monoclinic	monoclinic
a (Å)	23.038(5)	23.095(5)	15.309(3)	15.262(3)
b (Å)	15.004(3)	15.026(3)	21.861(4)	21.886(4)
c (Å)	23.183(5)	23.222(5)	21.336(4)	21.315(4)
β (deg)	100.18(3)	100.32(3)	108.74(3)	108.33(3)
V, Å^3	7888(3)	7928(3)	6727(2)	6758(2)
D(calcd), g·mm^{-1}	1.761	1.901	1.813	2.149
temp (°C)	25	25	25	25
λ, Mo Kα (Å)	0.71073	0.71073	0.71073	0.71073
μ (cm^{-1})	48.15	72.59	33.36	91.31
R1[a]	0.0379	0.0299	0.0496	0.0319
wR2[b]	0.0464	0.0398	0.1181	0.0571

[a] Conventional *R* on F_{hkl}: $\Sigma||F_o| - |F_c||/\Sigma|F_o|$. [b] Weighted *R* on $|F_{hkl}|^2$: $\{\sum[w(F_o^2 - F_c^2)^2]/\sum[w(F_o^2)^2]\}^{1/2}$.

positions and the ipso carbon were constrained to be equal. Additionally, the three methyl positions were constrained to be equidistant from each other.

Results and Discussion

Synthesis. We have previously reported that reaction of salicylic acid with triphenyl bismuth and niobium or tantalum ethoxide produces the complexes $Bi_2M_2(sal)_4(Hsal)_4(OEt)_4$ (M = Nb, Ta). Direct reaction of these complexes with stoichiometric amounts of water was found to produce a complex mixture of hydrolysis products that is difficult to separate. In contrast, the use of excess salicylic acid in the reaction mixture smoothly generates oxo complexes. The water of hydrolysis necessary for the reaction to proceed is believed to arise from an esterification reaction of the salicylic acid with liberated alcohol from the transition metal alkoxide. This type of reactivity has been frequently exploited to synthesize oxo-clusters of zirconium[19,20] and titanium,[21] and allowed for the isolation of the new complexes **1a** and **1b** as yellow or colorless crystals, respectively. These compounds have been characterized by single-crystal X-ray diffraction studies. Pertinent crystallographic details and selected bond lengths and angles are presented in Tables 1−3. Complexes **1a** and **1b** are isomorphous, and a representative diagram of **1a** is presented in Figures 1 and 2. Both complexes are found to lie on a crystallographic special position and possess C_2 symmetry in the solid-state. The geometry of the four metal atoms in the complex relative to one another is found to be intermediate between a square plane and a tetrahedron. In a square planar complex, the angle between the lines connecting the pairs of like atoms would be 0° (Figure 3A), whereas a tetrahedral orientation requires that the angle between those lines be 90° relative to one another (Figure 3B). In **1**, the angle between the line defined by the two bismuth atoms and the line defined by the M−O−M unit is approximately 70°, showing that there is significant distortion from either ideal configuration; however, the orientation of the metal atoms is closer to tetrahedral geometry than it is to square planar.

Table 2. Selected Bond Lengths [Å] and Angles [deg] for **1a**[a]

Bi(1)−O(43)	2.221(5)	Nb(2)−O(51)	1.829(5)
Bi(1)−O(23)#1	2.275(5)	Nb(2)−O(91)	1.9033(8)
Bi(1)−O(33)	2.299(5)	Nb(2)−O(21)	1.924(5)
Bi(1)−O(13)	2.490(6)	Nb(2)−O(11)	1.938(5)
Bi(1)−O(42)	2.500(6)	Nb(2)−O(12)	2.105(5)
Bi(1)−O(32)	2.639(6)	Nb(2)−O(22)	2.127(5)
Bi(1)−O(22)#1	2.738(5)		
O(43)−Bi(1)−O(23)#1	74.1(2)	O(43)−Bi(1)−O(22)#1	123.83(17)
O(43)−Bi(1)−O(33)	85.12(19)	O(23)#1−Bi(1)−O(22)#1	50.91(17)
O(23)#1−Bi(1)−O(33)	83.4(2)	O(33)−Bi(1)−O(22)#1	78.96(17)
O(43)−Bi(1)−O(13)	75.7(2)	O(13)−Bi(1)−O(22)#1	109.23(17)
O(23)#1−Bi(1)−O(13)	88.4(2)	O(42)−Bi(1)−O(22)#1	165.57(17)
O(33)−Bi(1)−O(13)	160.6(2)	O(32)−Bi(1)−O(22)#1	83.11(19)
O(43)−Bi(1)−O(42)	54.82(19)	O(51)−Nb(2)−O(91)	98.9(2)
O(23)#1−Bi(1)−O(42)	128.56(19)	O(51)−Nb(2)−O(21)	97.4(2)
O(33)−Bi(1)−O(42)	86.6(2)	O(91)−Nb(2)−O(21)	93.1(2)
O(13)−Bi(1)−O(42)	84.74(19)	O(51)−Nb(2)−O(11)	94.2(3)
O(43)−Bi(1)−O(32)	126.0(2)	O(91)−Nb(2)−O(11)	160.9(3)
O(23)#1−Bi(1)−O(32)	122.8(2)	O(21)−Nb(2)−O(11)	98.9(2)
O(33)−Bi(1)−O(32)	52.20(19)	O(51)−Nb(2)−O(12)	98.0(2)
O(13)−Bi(1)−O(32)	144.3(2)	O(91)−Nb(2)−O(12)	83.0(2)
O(42)−Bi(1)−O(32)	87.4(2)	O(21)−Nb(2)−O(12)	164.6(2)
O(11)−Nb(2)−O(12)	81.49(19)	O(11)−Nb(2)−O(22)	84.1(2)
O(51)−Nb(2)−O(22)	177.4(2)	O(12)−Nb(2)−O(22)	83.74(19)
O(91)−Nb(2)−O(22)	83.22(18)	Nb(2)−O(91)−Nb(2)#1	175.1(4)
O(21)−Nb(2)−O(22)	81.0(2)		

[a] Symmetry transformations used to generate equivalent atoms: #1 $-x + 1, y, -z + {}^1/_2$.

Under the conditions that were employed in the experiment, both complexes **1a** and **1b** cocrystallize with three molecules of toluene and a single molecule of water. The molecule of water observed in the solid-state structures of **1a** and **1b** is weakly bound to the bismuth atoms through the lone pairs of electrons on the oxygen atom (d_{Bi-O} = 3.018(9) Å). The water is well-defined in the crystal structure. Spectroscopic confirmation of the molecule of water was difficult due to the large number of residual hydroxyl groups that were associated with the salicylate ligands in the complexes. The coordination of water to bismuth in other heterobimetallic carboxylate complexes has been previously observed, and the $Bi-O_{water}$ bond distances that are observed in **1a** and **1b** agree well with these complexes.[12] In addition, the bond distances fall outside of the reported range for bridging oxo or hydroxo ligands between two bismuth centers.[22] The number and coordination modes of the

(19) Kickelbick, G.; Schubert, U. *J. Chem. Soc., Dalton Trans* **1999**, 1301−1305.
(20) Kickelbick, G.; Wiede, P.; Schubert, U. *Inorg. Chim. Acta* **1999**, *284*, 1−7.
(21) Kickelbick, G.; Schubert, U. **1998**, *198*, 159−161.

Table 3. Selected Bond Lengths [Å] and Angles [deg] for **1b**[a]

Bi(1)−O(43)	2.222(4)	Ta(1)−O(61)	1.833(5)
Bi(1)−O(13)	2.290(5)	Ta(1)−O(2)	1.9072(6)
Bi(1)−O(33)	2.307(5)	Ta(1)−O(11)	1.927(5)
Bi(1)−O(23A)	2.498(5)	Ta(1)−O(21)	1.956(5)
Bi(1)−O(42)	2.499(5)	Ta(1)−O(22)	2.081(4)
Bi(1)−O(32)	2.636(5)	Ta(1)−O(12)	2.121(4)
Bi(1)−O(12)	2.750(4)		
O(61)−Ta(1)−O(2)	98.3(2)	O(22)−Ta(1)−O(12)	83.78(17)
O(61)−Ta(1)−O(11)	96.2(2)	O(43)−Bi(1)−O(13)	74.48(17)
O(2)−Ta(1)−O(11)	93.00(19)	O(43)−Bi(1)−O(33)	85.19(17)
O(61)−Ta(1)−O(21)	95.0(2)	O(13)−Bi(1)−O(33)	83.43(18)
O(2)−Ta(1)−O(21)	161.9(2)	O(43)−Bi(1)−O(23A)	75.67(18)
O(11)−Ta(1)−O(21)	97.64(19)	O(13)−Bi(1)−O(23A)	87.86(18)
O(61)−Ta(1)−O(22)	98.7(2)	O(33)−Bi(1)−O(23A)	160.51(17)
O(2)−Ta(1)−O(22)	84.2(2)	O(43)−Bi(1)−O(42)	54.56(17)
O(11)−Ta(1)−O(22)	165.00(18)	O(13)−Bi(1)−O(42)	128.68(17)
O(21)−Ta(1)−O(22)	81.77(18)	O(33)−Bi(1)−O(42)	86.41(17)
O(61)−Ta(1)−O(12)	176.9(2)	O(23A)−Bi(1)−O(42)	85.50(17)
O(2)−Ta(1)−O(12)	83.72(16)	O(43)−Bi(1)−O(32)	126.38(19)
O(11)−Ta(1)−O(12)	81.27(18)	O(13)−Bi(1)−O(32)	122.13(18)
O(21)−Ta(1)−O(12)	83.51(19)	O(33)−Bi(1)−O(32)	52.16(18)
O(23A)−Bi(1)−O(32)	144.96(19)	O(23A)−Bi(1)−O(12)	108.27(15)
O(42)−Bi(1)−O(32)	88.02(18)	O(42)−Bi(1)−O(12)	165.64(16)
O(43)−Bi(1)−O(12)	123.76(16)	O(32)−Bi(1)−O(12)	82.88(16)
O(13)−Bi(1)−O(12)	50.35(14)	Ta(1)#1−O(2)−Ta(1)	172.9(4)
O(33)−Bi(1)−O(12)	79.24(15)	Ta(1)−O(12)−Bi(1)	136.82(19)

[a] Symmetry transformations used to generate equivalent atoms: #1 $-x$, y, $-z + {}^1/_2$.

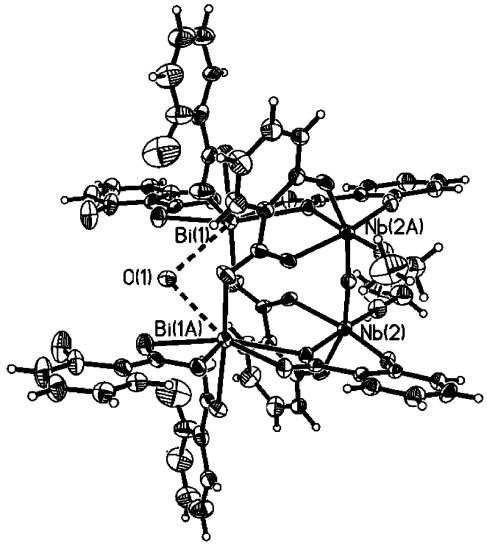

Figure 1. ORTEP representation of **1a**. Thermal ellipsoids are drawn at the 30% probability level for clarity. Coordinated water is represented by dashed lines. Symmetry equivalent atoms have letters in their labels.

salicylate and alkoxide ligands further precludes the oxygen atom from belonging to a charged oxide or hydroxide ion, and we would expect the Bi−O distances to be considerably shorter if this unit was a charged species.

The potential mechanisms resulting in the formation of **2a** and **2b** are less clear. The inclusion of magnesium acetate in the reaction was intended to produce a ternary metal salicylate complex; however, under no circumstances did we observe inclusion of the Mg^{2+} cation into a bimetallic compound, despite reports of stable magnesium−transition metal alkoxide/carboxylate systems.[10] The oxo ligands in the structure most likely are formed in a manner analogous to

(22) Hassan, A.; Breeze, S.; Courtenay, S.; Deslippe, C.; Wang, S. *Organometallics* **1996**, *15*, 5613−5621.

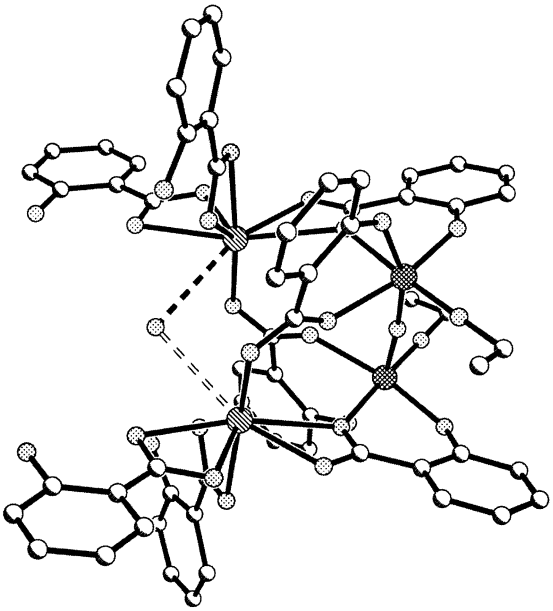

Figure 2. Ball-and-stick representation of compounds **1**. Bismuth atoms are represented with diagonal lines, while transition metal atoms are cross-hatched. Hydrogen atoms have been omitted for clarity. Coordinated water is illustrated with a dashed line.

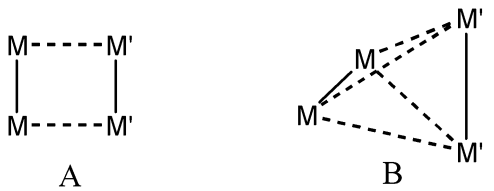

Figure 3. Line drawing representing the ideal orientations of four metal atoms in square planar (A) and tetrahedral (B) geometries.

that of complexes **1**, and it is possible that the magnesium acetate promotes the formation of water and/or the formation of oxo ligands by facilitating the esterification of salicylic acid. The presence of magnesium acetate in the reaction mixture is required for the formation of **2a** and **2b**. Repeated experiments using stoichiometric amounts of the reagents without the added magnesium acetate did not result in successful isolation of the desired complexes. Similarly, experiments that attempted to form the complexes using sodium acetate as opposed to magnesium acetate were unsuccessful. The differences in reactivity of the sodium and magnesium acetate may be tied to the preferred coordination number and charge of the respective cations, which may affect the formation of bimetallic complexes in solution. It is important to note that while the stable bimetallic complex incorporating magnesium has been reported, no such compounds incorporating the alkaline earth elements have been characterized. However, the exact manner in which the magnesium is interacting with the reaction mixture and helping to direct the formation of **2a** and **2b** is not completely understood at this point.

Complexes **2a** and **2b** crystallize from 2-propanol as yellow or colorless thin plates, respectively. Careful recrystallization of the compounds from a dichloromethane/hexane mixture results in the growth of large prisms, which were found to be identical to the thin plates. Pertinent crystallographic data and bond distances and angles are listed in

Table 4. Selected Bond Lengths [Å] and Angles [deg] for **2a**

Bi(1)−O(13)	2.205(19)	Nb(2)−O(4)	1.881(15)
Bi(1)−O(53)	2.326(19)	Nb(2)−O(41)	1.944(19)
Bi(1)−O(23)	2.352(17)	Nb(2)−O(42)	2.081(17)
Bi(1)−O(73)	2.536(6)	Nb(2)−O(63)	2.213(17)
Bi(1)−O(43)	2.598(17)	O(2)−Nb(4)	1.891(15)
Bi(1)−O(12)	2.67(2)	Nb(3)−O(81)	1.846(6)
Nb(1)−O(101)	1.851(6)	Nb(3)−O(4)	1.906(14)
Nb(1)−O(3)	1.880(16)	Nb(3)−O(3)	1.930(17)
Nb(1)−O(2)	1.903(15)	Nb(3)−O(71)	1.944(19)
Nb(1)−O(21)	1.944(17)	Nb(3)−O(72)	2.082(16)
Nb(1)−O(22)	2.118(17)	Nb(3)−O(33)	2.151(17)
Nb(1)−O(32)	2.204(18)	Nb(4)−O(111)	1.810(18)
O(1)−Nb(4)	1.890(16)	Nb(4)−O(51)	1.953(17)
O(1)−Nb(2)	1.914(16)	Nb(4)−O(52)	2.133(18)
Nb(2)−O(91)	1.854(6)	Nb(4)−O(62)	2.174(18)
O(13)−Bi(1)−O(53)	81.8(7)	O(23)−Bi(1)−O(43)	149.1(6)
O(13)−Bi(1)−O(23)	85.0(7)	O(73)−Bi(1)−O(43)	127.7(5)
O(53)−Bi(1)−O(23)	74.2(6)	O(13)−Bi(1)−O(12)	52.6(6)
O(13)−Bi(1)−O(73)	85.0(5)	O(53)−Bi(1)−O(12)	125.5(6)
O(53)−Bi(1)−O(73)	146.8(5)	O(23)−Bi(1)−O(12)	122.0(6)
O(23)−Bi(1)−O(73)	74.4(5)	O(73)−Bi(1)−O(12)	65.4(4)
O(13)−Bi(1)−O(43)	77.0(6)	O(43)−Bi(1)−O(12)	64.6(6)
O(53)−Bi(1)−O(43)	78.5(6)	O(101)−Nb(1)−O(3)	101.1(5)
O(101)−Nb(1)−O(2)	99.3(5)	O(4)−Nb(2)−O(63)	168.3(6)
O(3)−Nb(1)−O(2)	94.6(7)	O(1)−Nb(2)−O(63)	82.3(6)
O(101)−Nb(1)−O(21)	90.3(5)	O(41)−Nb(2)−O(63)	80.6(7)
O(3)−Nb(1)−O(21)	160.1(7)	O(42)−Nb(2)−O(63)	80.0(7)
O(2)−Nb(1)−O(21)	99.7(7)	Nb(4)−O(2)−Nb(1)	145.4(10)
O(101)−Nb(1)−O(22)	167.9(5)	O(81)−Nb(3)−O(4)	97.7(5)
O(3)−Nb(1)−O(22)	87.6(7)	O(81)−Nb(3)−O(3)	97.7(5)
O(2)−Nb(1)−O(22)	88.3(6)	O(4)−Nb(3)−O(3)	93.9(7)
O(21)−Nb(1)−O(22)	79.1(7)	O(81)−Nb(3)−O(71)	96.2(6)
O(101)−Nb(1)−O(32)	89.5(5)	O(4)−Nb(3)−O(71)	101.0(7)
O(3)−Nb(1)−O(32)	83.1(7)	O(3)−Nb(3)−O(71)	158.0(7)
O(2)−Nb(1)−O(32)	171.2(7)	O(81)−Nb(3)−O(72)	173.2(5)
O(21)−Nb(1)−O(32)	80.6(7)	O(4)−Nb(3)−O(72)	88.6(7)
O(22)−Nb(1)−O(32)	83.1(6)	O(3)−Nb(3)−O(72)	84.4(7)
Nb(4)−O(1)−Nb(2)	154.7(8)	O(71)−Nb(3)−O(72)	80.0(7)
O(91)−Nb(2)−O(4)	101.0(5)	O(81)−Nb(3)−O(33)	90.1(5)
O(91)−Nb(2)−O(1)	101.3(5)	O(4)−Nb(3)−O(33)	171.8(7)
O(4)−Nb(2)−O(1)	93.1(6)	O(3)−Nb(3)−O(33)	82.5(7)
O(91)−Nb(2)−O(41)	88.9(6)	O(71)−Nb(3)−O(33)	80.6(7)
O(4)−Nb(2)−O(41)	101.8(7)	O(72)−Nb(3)−O(33)	83.7(6)
O(1)−Nb(2)−O(41)	160.1(7)	Nb(1)−O(3)−Nb(3)	153.8(9)
O(91)−Nb(2)−O(42)	166.0(5)	O(111)−Nb(4)−O(1)	98.6(7)
O(4)−Nb(2)−O(42)	89.1(7)	O(111)−Nb(4)−O(2)	100.0(7)
O(1)−Nb(2)−O(42)	87.7(7)	O(1)−Nb(4)−O(2)	95.5(7)
O(41)−Nb(2)−O(42)	79.5(7)	O(111)−Nb(4)−O(51)	94.7(8)
O(91)−Nb(2)−O(63)	90.4(5)	O(1)−Nb(4)−O(51)	159.1(7)
O(2)−Nb(4)−O(51)	98.0(7)	O(1)−Nb(4)−O(62)	83.4(7)
O(111)−Nb(4)−O(52)	170.5(7)	O(2)−Nb(4)−O(62)	169.1(7)
O(1)−Nb(4)−O(52)	84.8(7)	O(51)−Nb(4)−O(62)	80.3(7)
O(2)−Nb(4)−O(52)	88.4(7)	O(52)−Nb(4)−O(62)	80.7(7)
O(51)−Nb(4)−O(52)	79.7(7)	Nb(2)−O(4)−Nb(3)	149.5(9)
O(111)−Nb(4)−O(62)	90.9(7)		

Table 5. Selected Bond Lengths [Å] and Angles [deg] for **2b**

Bi(1)−O(43)	2.240(6)	Ta(2)−O(4)	1.897(5)
Bi(1)−O(63)	2.337(6)	Ta(2)−O(21)	1.973(6)
Bi(1)−O(73)	2.348(6)	Ta(2)−O(22)	2.068(6)
Bi(1)−O(53)	2.554(7)	Ta(2)−O(33)	2.170(7)
Bi(1)−O(23)	2.588(7)	O(2)−Ta(4)	1.892(6)
Bi(1)−O(42)	2.655(6)	O(3)−Ta(3)	1.898(5)
Ta(1)−O(81)	1.834(5)	O(3)−Ta(4)	1.905(5)
Ta(1)−O(4)	1.901(5)	Ta(3)−O(111)	1.837(6)
Ta(1)−O(2)	1.904(6)	Ta(3)−O(51)	1.953(5)
Ta(1)−O(61)	1.958(6)	Ta(3)−O(52)	2.082(6)
Ta(1)−O(62)	2.132(5)	Ta(3)−O(13)	2.143(6)
Ta(1)−O(32)	2.163(7)	Ta(4)−O(101)	1.834(6)
O(1)−Ta(2)	1.887(6)	Ta(4)−O(71)	1.953(5)
O(1)−Ta(3)	1.913(6)	Ta(4)−O(72)	2.106(5)
Ta(2)−O(91)	1.844(6)	Ta(4)−O(12)	2.178(6)
O(43)−Bi(1)−O(63)	81.5(2)	O(53)−Bi(1)−O(23)	126.1(2)
O(43)−Bi(1)−O(73)	84.6(2)	O(43)−Bi(1)−O(42)	54.8(2)
O(63)−Bi(1)−O(73)	74.8(2)	O(63)−Bi(1)−O(42)	126.8(2)
O(43)−Bi(1)−O(53)	85.0(2)	O(73)−Bi(1)−O(42)	122.5(2)
O(63)−Bi(1)−O(53)	147.6(2)	O(53)−Bi(1)−O(42)	64.2(2)
O(73)−Bi(1)−O(53)	74.7(2)	O(23)−Bi(1)−O(42)	64.2(2)
O(43)−Bi(1)−O(23)	77.9(2)	O(81)−Ta(1)−O(4)	98.6(2)
O(63)−Bi(1)−O(23)	79.6(2)	O(81)−Ta(1)−O(2)	99.7(2)
O(73)−Bi(1)−O(23)	150.8(2)	O(4)−Ta(1)−O(2)	95.7(2)
O(81)−Ta(1)−O(61)	94.7(2)	O(21)−Ta(2)−O(33)	81.1(2)
O(4)−Ta(1)−O(61)	158.9(2)	O(22)−Ta(2)−O(33)	80.7(2)
O(2)−Ta(1)−O(61)	98.1(2)	Ta(4)−O(2)−Ta(1)	146.0(3)
O(81)−Ta(1)−O(62)	171.2(2)	Ta(3)−O(3)−Ta(4)	154.7(3)
O(4)−Ta(1)−O(62)	84.9(2)	O(111)−Ta(3)−O(3)	98.5(2)
O(2)−Ta(1)−O(62)	87.9(2)	O(111)−Ta(3)−O(1)	98.0(3)
O(61)−Ta(1)−O(62)	79.8(2)	O(3)−Ta(3)−O(1)	95.3(2)
O(81)−Ta(1)−O(32)	91.5(3)	O(111)−Ta(3)−O(51)	94.9(2)
O(4)−Ta(1)−O(32)	82.6(2)	O(3)−Ta(3)−O(51)	158.4(2)
O(2)−Ta(1)−O(32)	168.8(2)	O(1)−Ta(3)−O(51)	99.6(2)
O(61)−Ta(1)−O(32)	80.7(2)	O(111)−Ta(3)−O(52)	172.2(3)
O(62)−Ta(1)−O(32)	80.9(2)	O(3)−Ta(3)−O(52)	84.9(2)
Ta(2)−O(1)−Ta(3)	148.1(3)	O(1)−Ta(3)−O(52)	88.7(2)
O(91)−Ta(2)−O(1)	100.7(2)	O(51)−Ta(3)−O(52)	79.9(2)
O(91)−Ta(2)−O(4)	100.9(2)	O(111)−Ta(3)−O(13)	90.6(3)
O(1)−Ta(2)−O(4)	94.1(2)	O(3)−Ta(3)−O(13)	81.7(2)
O(91)−Ta(2)−O(21)	89.7(2)	O(1)−Ta(3)−O(13)	171.2(2)
O(1)−Ta(2)−O(21)	100.8(2)	O(51)−Ta(3)−O(13)	81.2(2)
O(4)−Ta(2)−O(21)	159.9(2)	O(52)−Ta(3)−O(13)	82.9(2)
O(91)−Ta(2)−O(22)	166.7(3)	O(101)−Ta(4)−O(2)	99.9(2)
O(1)−Ta(2)−O(22)	88.9(2)	O(101)−Ta(4)−O(3)	100.0(2)
O(4)−Ta(2)−O(22)	87.5(2)	O(2)−Ta(4)−O(3)	95.1(2)
O(21)−Ta(2)−O(22)	79.4(2)	O(101)−Ta(4)−O(71)	90.7(2)
O(91)−Ta(2)−O(33)	90.2(2)	O(2)−Ta(4)−O(71)	100.0(2)
O(1)−Ta(2)−O(33)	168.9(2)	O(3)−Ta(4)−O(71)	159.7(2)
O(4)−Ta(2)−O(33)	81.8(2)	O(101)−Ta(4)−O(72)	168.1(2)
O(2)−Ta(4)−O(72)	88.5(2)	O(3)−Ta(4)−O(12)	81.7(2)
O(3)−Ta(4)−O(72)	87.5(2)	O(71)−Ta(4)−O(12)	81.4(2)
O(71)−Ta(4)−O(72)	79.5(2)	O(72)−Ta(4)−O(12)	82.8(2)
O(101)−Ta(4)−O(12)	89.1(2)	Ta(2)−O(4)−Ta(1)	155.8(3)
O(2)−Ta(4)−O(12)	170.9(2)		

Tables 1, 4, and 5. The complexes were found to be isomorphous. A representative ORTEP diagram of the molecules is shown in Figures 4 and 5. The structures consist of a tetrameric M_4O_4 ring system completed by bridging and chelating carboxylate ligands. A single bismuth−salicylate unit caps the transition metal tetramer.

The shortest transition metal−oxygen bonds in all of the complexes discussed in this paper are associated with the terminal alkoxide ligands and range from 1.810(8) to 1.914(16) Å. The metal−oxo ligand bond distances were only slightly larger than these values and range from 1.880(16) to 1.914(16) Å. The longest bonds in the octahedral transition metal coordination environment were found to be associated with the salicylate ligands. The metal−phenolic oxygen bond distances range from 1.924(5) to 1.973(6) Å, while the metal−carboxylate oxygen bond distances are longer (2.068(6)−2.213(17) Å). In all cases, the longest bonds in the transition metal coordination environment were oriented *trans* to the shortest bonds. The values for the transition metal−oxygen bond distances were in excellent agreement with similar complexes that have been previously reported.[12,23] The bismuth atoms in complexes **1** are eight coordinate and adopt a roughly pentagonal bipyramidal geometry. In complexes **2**, the bismuth atoms are found to be five coordinate and can be described as having an almost ideal square pyramidal geometry. A much weaker sixth

(23) Hubert-Pfalzgraf, L. G.; Abada, V.; Halut, S.; Roziere, J. *Polyhedron* **1997**, *16*, 581−585.

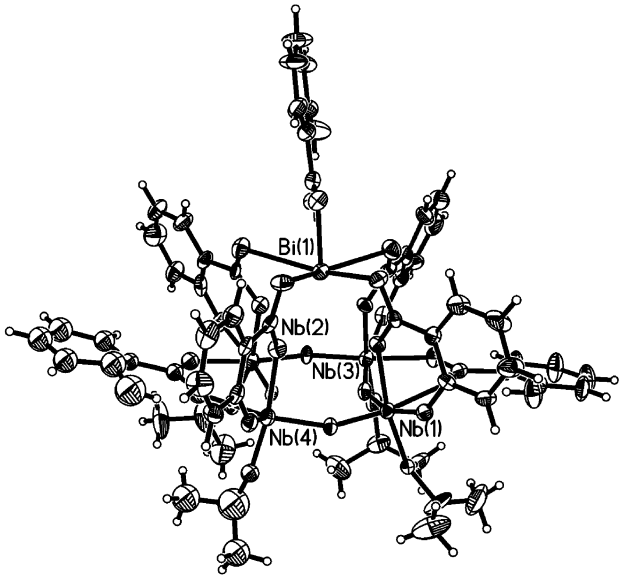

Figure 4. ORTEP representation of **2a**. Thermal ellipsoids are drawn at the 30% probability level for clarity. Only one orientation of the disordered 2-propoxide ligand is shown.

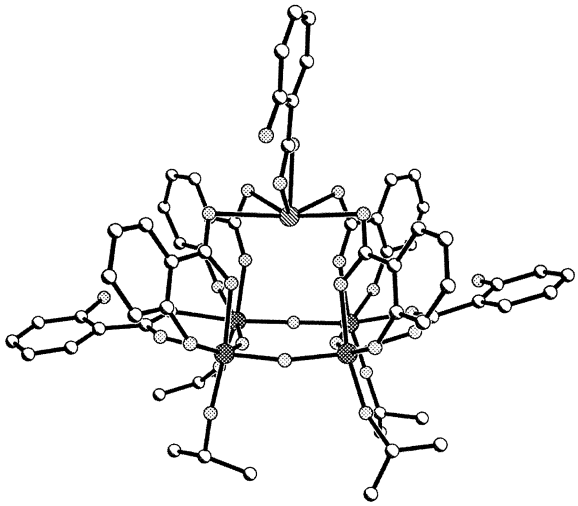

Figure 5. Ball-and-stick representation of compounds **2**. Bismuth atoms are represented with diagonal lines, while transition metal atoms are cross-hatched. Hydrogen atoms have been omitted for clarity. Coordinated water is illustrated with a dashed line.

interaction is present between the metal center and the second oxygen atom of the terminal salicylate ligand (d_{Bi-O} = 2.655(6)−2.67(2) Å). This bond distance is significantly longer than that of the oxygen formally bound to the bismuth center (d_{Bi-O} = 2.205(19)−2.240(6) Å), and is clearly much weaker than the other Bi−O carboxylate bonds. Excluding the coordinated water, which has been discussed previously, the bismuth−oxygen bond distances in **1a** and **1b** range from 2.221(5) to 2.750(4) Å. The bismuth−oxygen bond distances in **2a** and **2b** are similar, ranging from 2.205(19) Å to 2.67(2) Å. There is a general trend, similar to the transition metals, that the longest bonds are oriented *trans* to the shortest ones. However, the geometry at the bismuth center is distorted to the point that it is difficult to draw many conclusions from this observation.

NMR studies of the complexes discussed in this paper reveal the presence of a single salicylate environment in solution, despite the observation of multiple ligand environments in the solid-state. This observation strongly suggests that the salicylate ligands of these complexes are fluxional and undergo an exchange process that is fast on the NMR time scale, resulting in the detection of only a single ligand environment.

The effective molar mass of complex **1b** was determined by a vapor diffusion experiment between a solution of the compound and that of a known concentration of tetraphenyl lead. Due to the NMR results, we suspected that **1b** could dissociate in solution, so the concentration of tetraphenyl lead was chosen so that its vapor pressure would lie between that of a theoretical solution of **1b** that did not dissociate and one that would dissociate into two or more ions. The starting concentration of tetraphenyl lead was 17 mM, and after equilibration, it was found to be 16.8 mM, which should correspond to the total concentration of all species in the solution of **1b**. If the molecule does not dissociate, then the molar mass determined from the solution data is 1071 g·mol^{-1}. This value is significantly different from the expected molar mass for intact **1b** (1978 g·mol^{-1}). Assuming dissociation into the two noted particles (van't Hoff *i*-factor equals 2), the calculated molar mass is 2142 g·mol^{-1}. This agrees well with the value calculated from the solid-state structure of **1b**. It seems likely that the ability of the complex to dissociate into ions in solution is also responsible for the observed exchange of salicylate ligands in the NMR spectra. If dissociation were to occur, one likely set of ions to be formed would be a $Bi(Hsal)_2^+$ cation and a $BiNb_2(\mu\text{-}O)(Hsal)_2(sal)_4(OEt)_2^-$ anion.

Thermal and Hydrolytic Behavior. The thermal decompositions of compounds **1a** and **1b** were examined by TGA and by powder X-ray diffraction. The molecular complexes can be cleanly converted to the desired heterobimetallic oxides by heating in air. TGA analysis of the thermal decomposition of the molecules reveals that the compounds decompose in two steps to produce the final bimetallic oxide on heating in air to approximately 375 °C (Figure 6). The initial mass loss of volatile material from the sample is likely caused by the elimination of lattice solvent and water from the sample, along with a small amount of possible hydrolysis of the residual alkoxide ligands. There was a 60.4% and 55.0% mass loss during the pyrolysis of **1a** and **2a**, respectively. These values are in good agreement with the calculated mass losses of 61.5% and 54.5% that are required for the conversion of the molecular precursors to the corresponding bimetallic oxide. Differential thermal analysis (DTA) studies of these complexes during pyrolysis revealed that there is an exothermic peak immediately prior to the formation of the final oxide. We have assigned this peak to a phase change in the oxide lattice, as essentially no mass is lost during the event.

Powder X-ray diffraction studies of the final products produced from the TGA studies at 500 °C revealed those materials to be amorphous. Stronger heating of the samples, using temperatures in excess of 600 °C during calcination, was required for crystallization. These results agree with previous observations for the formation of bismuth-based

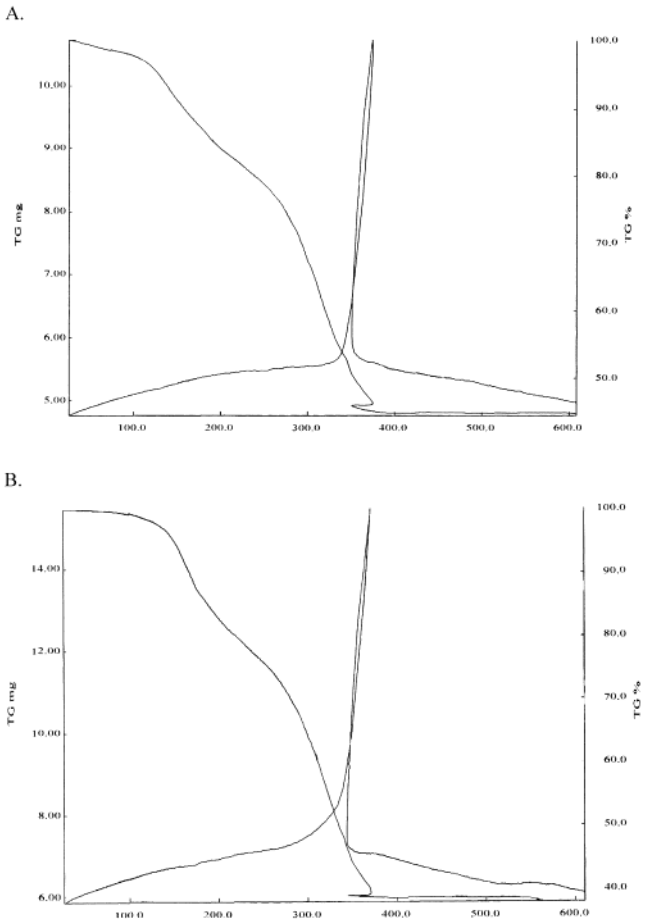

Figure 6. TGA/DTA trace of the thermal decomposition of **1a** (A) and **1b** (B) in air.

materials using sol−gel techniques.[25] The effects of the time and temperature of the sintering process on the phases present in the oxide of **1a** have been investigated (Figure 7). In all cases, the complexes decomposed on heating in air to produce the metastable high temperature form of $BiNbO_4$ as the major crystalline phase, in agreement with the composition predicted by the binary phase diagrams reported for the bismuth−niobium oxide systems (Figure 8).[26,27] Sintering a sample of **1a** for 2 h at 650 °C produces only the anticipated product $BiNbO_4$. The product from this reaction was unexpectedly found to be primarily composed of the metastable high temperature form of $BiNbO_4$ ($BiNbO_4$-H), which has a triclinic unit cell. The balance of the material was found to be the low temperature form the bimetallic oxide, $BiNbO_4$-L, which has an orthorhombic unit cell. Under the conditions already detailed, the two phases in the material were found to be present in an approximately 4:1 ratio. Increasing the temperature of the sintering process favors conversion of $BiNbO_4$-H into $BiNbO_4$-L, along with concomitant disproportionation of the bimetallic oxide into

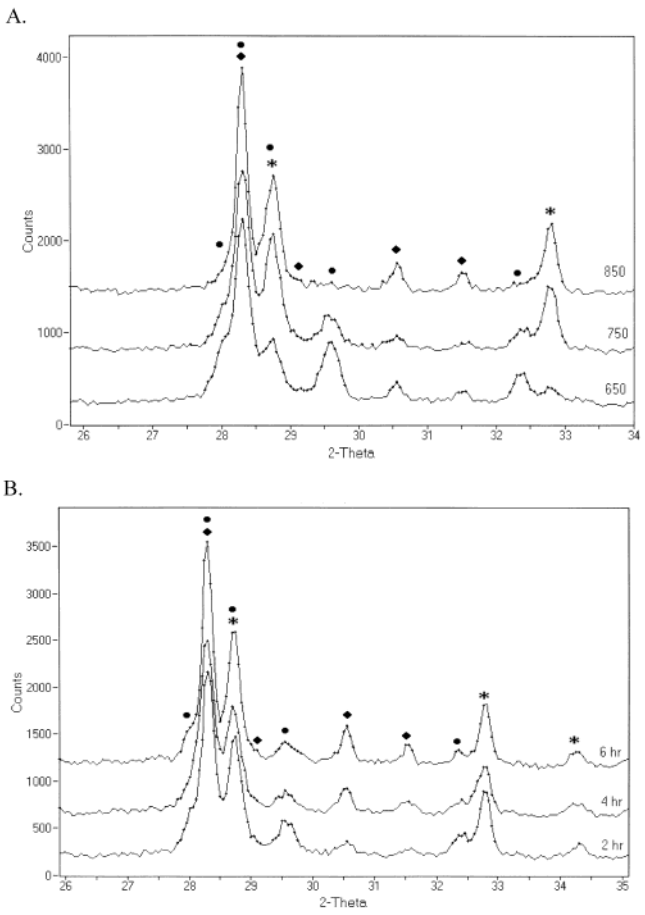

Figure 7. Powder X-ray diffraction pattern of the oxide of **1a** produced from various calcination temperatures for 2 h (A) and from calcination at 750 °C for various lengths of time (B). The phases present are $BiNbO_4$-H (●), $BiNbO_4$-L (◆), and $Bi_5Nb_3O_{15}$ (*).

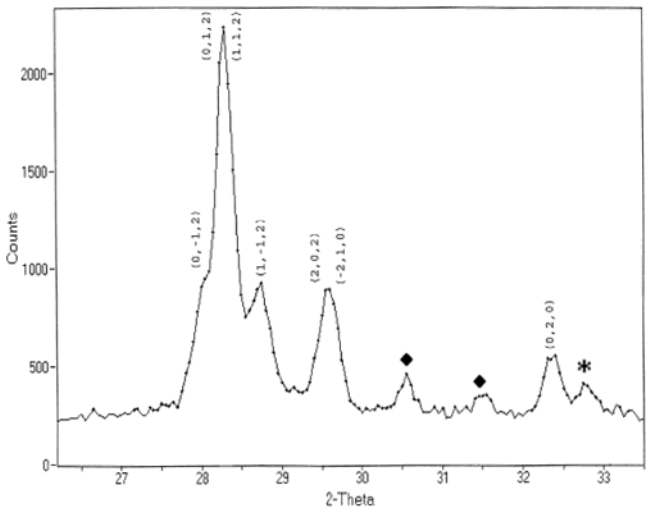

Figure 8. Indexed powder X-ray diffraction pattern of the oxide of **1a** produced after heating the molecular precursor for 2 h at 650 °C in air. Indexed peaks relate to the high temperature (triclinic) phase of $BiNbO_4$. Peaks marked with ◆ relate to the low temperature (orthorhombic) phase of the same material, while peaks marked with * relate to $Bi_5Nb_3O_{15}$.

$Bi_5Nb_3O_{15}$ and Nb_2O_5. Similarly, increasing the sintering time of the sample was found to favor the conversion of $BiNbO_4$-H into $BiNbO_4$-L, although to a smaller extent. Upon either increasing the reaction temperature from 650 °C to 850 °C or the reaction time from 2 to 6 h, the (0,4,0) and

(24) Steunou, N.; Bonhomme, C.; Sanchez, C.; Vaissermann, J.; Hubert-Pfalzgraf, L. G. *Inorg. Chem.* **1998**, *37*, 901.
(25) Zhou, Q. F.; Chan, H. L. W.; Choy, C. L. *J. Non-Cryst. Solids* **1999**, *254*, 106−111.
(26) Roth, R. S.; Waring, J. *J. Res. Natl. Bur. Stand. (U.S.)* **1962**, *66A*, 451−463.
(27) Ling, C. D.; Withers, R. L.; Schmid, S.; Thompson, J. G. *J. Solid State Chem.* **1998**, *137*, 42−61.

the (0,0,2) reflections of the $BiNbO_4$-L phase increase in intensity and sharpness, while the overlapping (2,0,2) and (2,1,0) reflections of the $BiNbO_4$-H become more diffuse or disappear entirely. These results suggest that the initial formation of $BiNbO_4$ is kinetically controlled. However, once the bimetallic oxide is formed, the thermodynamically more stable $BiNbO_4$-L is favored, and continued reaction and crystallization of the material will favor the formation of this product at the expense of the $BiNbO_4$-H. This behavior has been observed in several other binary oxide systems that are produced using classical or modified sol−gel techniques.[28,29]

As mentioned previously, extended reaction of the $BiNbO_4$-H results in the disproportionation to $Bi_5Nb_3O_{15}$ and Nb_2O_5 as well as conversion to $BiNbO_4$-L. It seems likely that the disproportionation products are formed from $BiNbO_4$-H. However, at this point it is not clear whether these products form directly from $BiNbO_4$-H, or form via the intermediacy of $BiNbO_4$-L, or, possibly, by both pathways. It does appear, however, that $Bi_5Nb_3O_{15}$ and Nb_2O_5 do not result directly from conversion of the molecular precursor **1a**. Other possible pathways for the formation of the disproportionation products involving either volatilization of bismuth oxide during decomposition of the molecular precursor or possible reaction of the oxide mixture with the ceramic crucible to form a sillenite-related phase of approximate composition $Bi_{12}Nb_{0.29}O_{18.7-x}$ are possible but were not observed here.[27] We have found that sintering the samples at temperatures of 600 °C effectively inhibits the production of disproportionation products and $BiNbO_4$-L, and $BiNbO_4$-H is produced as the only crystalline phase. These results agree with other findings on the formation of metastable states in bimetallic oxide systems and suggest that crystallite growth and grain size may be important in determining the oxide phase that is formed.[29] It is important to note that the use of the molecular complex **1a** allows for the formation of crystalline $BiNbO_4$-H at temperatures of 650 °C in 2 h. In contrast, reported solid-state syntheses require sintering periods of 24−240 h at 1173 °C to achieve the high temperature form of the bimetallic oxide product.[27]

BET, SEM, and EDX have been used to study the morphology of the oxides produced from the thermal decomposition of **1a** and **1b**. Pyrolysis of the solid-state compounds produces a porous oxide, probably owing to the concomitant high energy of the reaction environment and oxidation of the organic ligands. SEM analysis of the materials produced in this manner reveals the presence of numerous pores and channels permeating the oxide (Figure 9). BET analysis reveals that the surface areas of the oxides of **1a** and **1b** are 3.99 and 6.62 m^2/g, respectively. These results indicate that the majority of the pores in the oxide are macroscopic, characteristic of a material with a very low density and possessing a relatively low surface area.

Bimetallic oxides are also achievable through hydrolysis of the molecular precursors in the presence of $[Et_4N]OH$ in refluxing H_2O. SEM analysis of the hydrolysis product reveals this method produces particles with diameters ranging from 152 to 197 nm and an average diameter of approximately 174 nm (Figure 10). These particles are well below the 250 nm dimensions that are required to produce ferroelectric oxides. The particles synthesized in this manner can be dispersed repeatedly in a wide variety of solvents through sonication, provided that the oxide is not dried completely on isolation. Once dried, the particles show a significant tendency to aggregate and become difficult to redisperse, suggesting that this may be an accessible route to stable thin films of ferroelectric materials.

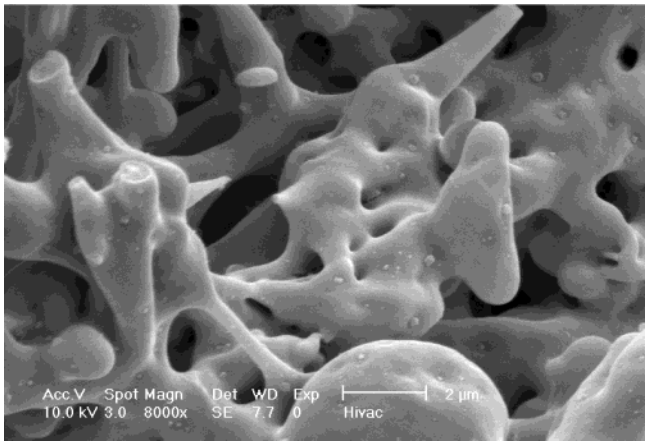

Figure 9. SEM image of the bulk pyrolysis product of **1a** produced after 2 h at 750 °C.

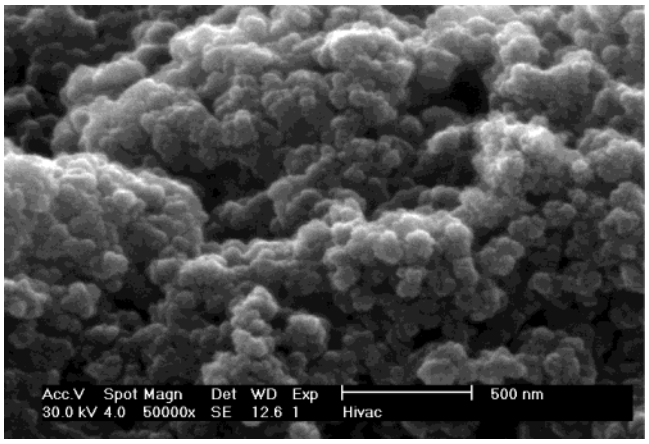

Figure 10. SEM image of the aggregated hydrolysis product of **1b**.

Conclusion

Heterobimetallic complexes of bismuth can be synthesized in a stepwise manner if careful control is paid to the nature of the organic ligand that is employed in the synthesis and to the reaction conditions that are used in the formation of the product. The products display influences of the coordinative flexibility of the salicylate ligands, the relative solubility of the bimetallic products in a given solvent system, the oxidation state of the transition metal, the tendency of the transition metal to remain octahedral, and the ability of bismuth to easily expand its coordination sphere. It seems likely that the cumulative effects of these traits, acting in

(28) Gopalakrishnan, J. *Chem. Mater.* **1995**, *7*, 1265−75.
(29) Mather, S. A.; Davies, P. K. *J. Am. Ceram. Soc.* **1995**, *78*, 2737−45.
(30) Soltek, R. *Winray GL*; Zurük zum Anorganisch-Chemischen Institut: Heidelberg, Germany, 2000.

concert, are what ultimately determine the composition and structure of the bimetallic complexes.

The compounds synthesized in this manuscript are found to cleanly decompose under hydrolysis or thermolysis to produce bimetallic oxides. The conditions required to produce bimetallic oxides from these molecular precursors are significantly milder than what has been previously reported, which opens the possibility of new routes to interesting and potentially useful metastable bismuth oxide phases. The high solubility of these complexes in common organic solvents, coupled with their ease of decomposition, could make them attractive precursors to the synthesis of bimetallic and multimetallic oxide films and coatings using a variety of techniques.

Crystallographic data for the complexes discussed in this paper has been deposited with the Cambridge Crystallographic Data Center (CCDC), No. 202936-202939. Copies of this information may be obtained free of charge from The Director, CCDC, 12 Union Road, Cambridge CB2 1EZ, U.K. (Fax: 44-1233-336-033. E-mail: deposit@ccdc.cam.ac.uk; www: http://www.ccdc.cam.ac.uk.)

Acknowledgment. This work was supported by grants from the Robert A. Welch Foundation and from the Unites States National Science Foundation. J.H.T. wishes to thank Elizabeth Whitsett for assistance with collection of SEM images and EDX data.

Supporting Information Available: Crystallographic information in CIF format and completely labelled diagrams of the complexes, including those not presented in the text of this article. This material is available free of charge via the Internet at http://pubs.acs.org.

IC026108S